Radar Data Clustering and Bounding Box Estimation with Doppler Measurements

J. Zeng
McMaster University
Hamilton, Canada
zengj41@mcmaster.ca

P. Mannari
McMaster University
Hamilton, Canada
mannarip@mcmaster.ca

A. Acharya
Uhnder, Inc
Toronto, Canada
aalok.acharya@uhnder.com

R. Tharmarasa
McMaster University
Hamilton, Canada
thamas@mcmaster.ca

***Abstract*—High-resolution automotive radars, which are widely used nowadays, yield multiple measurements per frame from a single target. Clustering these measurements accurately and finding the tight bounding boxes are two challenging problems. In this work, the shape is estimated using a rectangular bounding box using the position and range rate measurements from the radar. While the Doppler (or range rate) measurements provide extra information about the target velocity, the presence of micro-Doppler (for example, returns from tires of a car) can significantly degrade the clustering, bounding box and heading estimates. It is necessary to cluster the measurements corresponding to different targets, as well as those that occur due to micro-Doppler. A clustering method is developed that can effectively use the Doppler information to differentiate closely spaced targets while avoiding the drawbacks of micro-Doppler. The bounding box estimate is refined by using only the measurements corresponding to the target bulk and, in turn, further aids in clustering iteratively. The effectiveness of the proposed approach is verified using simulations for different scenarios.**

***Index Terms*—Clustering, autonomous vehicle, micro-Doppler, radar data, extended target**

I. Introduction

Nowadays, radars are indispensable for environmental understanding in autonomous driving because of their cost-effectiveness and perception capabilities in all-weather conditions [1]. Radars usually provide multiple detections, including range, azimuth and Doppler measurements from each nearby object, such that the location, velocity and shape of the object can be estimated from these detections. In contrast to point targets, which are usually considered in the tracking algorithms, such objects have non-negligible shapes and are known as extended targets [2].

Clustering radar measurements and estimating the bounding boxes of each cluster are necessary steps for subsequent object tracking and environmental understanding. By dividing radar measurements into different clusters corresponding to different targets and obtaining bounding boxes for each cluster, the location, orientation and size of each target could be estimated. The extended targets could be converted into point targets by considering their bounding box center as their location and could be tracked with classical tracking algorithms [3].

Some of the widely used clustering methods for radar measurements include Density-Based Spatial Clustering of Applications with Noise (DBSCAN) [4] and K-Means Clustering [5], and Doppler information is usually considered in radar data clustering. A multi-stage clustering framework utilizing velocity information for filtering and clustering radar data is presented in [6]. Wagner et al. consider range, Doppler, and direction of arrival (DoA) measurements from radar as multi-dimensional data and cluster them with Ellipsoid DBSCAN method [7]. In [8], the inputs are clustered according to range and velocity difference first, then K-Means algorithm is applied to adjust clusters. In [9], bounding box estimation is performed by iterating through all possible orientations of the box and fitting the box to the measurements according to different criteria, such as area minimization or variance maximization.

However, most of the radar data clustering regarding Doppler information cannot handle the problem caused by the micro-Doppler effect. Besides the translation of targets, the micro-motion dynamics of any structure on targets, e.g., mechanical rotation and vibration, also induce Doppler modulation in the returned signal, which is referred to as the micro-Doppler effect [10]. The range rates of radar measurements from target structures with micro-motion have large differences from that of other measurements from the same target due to the micro-Doppler effect. Thus, they may be separated from other measurements from the same target or clustered with measurements from other targets with the same range rate, which leads to errors in clustering and has negative impacts on subsequent pose estimation and tracking. In [11], a grid-based clustering is proposed to handle the micro-Doppler effect induced by the micro-motion of the pedestrian body. However, the literature on radar data clustering considering micro-Doppler due to vehicle tire rotation is limited.

The current work deals with the problem of clustering and bounding box estimation using Doppler measurements which include those due to micro-Doppler effects due to rotation of the tires. The objective is to form clusters that correspond to the target body (no micro-Doppler effect) for multiple targets and to integrate/merge measurements from the tires to the corresponding target cluster. The speed and heading of each cluster are estimated for each cluster using the measurements from the target body/bulk. The bounding box is estimated to fit the measurements from the target body for each cluster, using the heading estimate as the prior. The clustering and the bounding box estimation are performed iteratively, i.e., the

current cluster is refined using the estimated bounding box and its range rate distribution to include relevant measurements from the body and the tires and the bounding box estimate is further updated using the newly formed cluster. In this manner, the proposed approach can utilize the range rate information for clustering and bounding box estimation while rejecting the negative effects due to micro-Doppler.

The main contributions of the paper are

1) Derivation of iterative least squares method for speed and heading estimation using range rate and azimuth measurements.
2) MAP (maximum a posterior) method for bounding box estimation aided by the heading estimate.
3) Derivation of p.d.f of micro-Doppler effect due to tire rotation.
4) Clustering of targets while handling measurements due to micro-Doppler.

The notations used in this article are as follows: Uppercase bold letters are used to denote matrices, lowercase bold letters are used to denote vectors, scalars are denoted by normal lowercase letters and normal uppercase letters are used to denote random variables.

Section II of the paper contains the mathematical description of the problem and the models used. Section III describes the procedure for L-fitting / bounding box estimation and the effect due to micro-Doppler is quantified in Section IV. The proposed two-step clustering method is described in Section V. The simulation results are presented in Section VI and finally, Section VII provides the conclusions and directions for future work.

II. System and Measurements Models

Using Doppler measurements along with the normal position measurements can lead to improvement in the clustering of closely spaced targets as well as better bounding box estimation for each target. However, due to micro-Doppler effects, a naive clustering approach can incorrectly cluster micro-Doppler measurements along with those from the target body or form extra clusters for the micro-Doppler measurements. The performance of clustering and the estimates of the headings and the bounding boxes are severely degraded if micro-Doppler measurements are included along with the normal measurements. Hence, the objective of this work is two-fold:

1. Form clusters for each target (maybe closely spaced) while differentiating measurements from the body and tires.
2. Estimate bounding box for each cluster with effective use of Doppler data.

The following assumption is made in this work:

1. The heading of a vehicle is the same as the direction of its velocity.
2. Only the range, azimuth and range-rate measurements are used for clustering and bounding box estimates. Elevation measurements, if available, can be used to find the height of the boxes.

A. System and Measurements Models

The radar coordinate system is defined as a right-handed coordinate system. Its origin is the position of the radar, and the positive direction of y axis points directly ahead of the radar.

The state of an arbitrary scattering point P (from a tire of the vehicle or the body) and the radar sensor in the world coordinate, at k^{th} time step, are denoted as $\mathbf{x}_k^w = [x_k^w, \dot{x}_k^w, y_k^w, \dot{y}_k^w]^T$ and $\mathbf{x}_k^{ws} = [x_k^{ws}, \dot{x}_k^{ws}, y_k^{ws}, \dot{y}_k^{ws}]^T$, respectively. The superscript w, s and $(\cdot)^T$ denote the world coordinate, radar sensor and the mathematical transpose operation, respectively. Then, the state of point P in the radar coordinate system $\mathbf{x}_k = [x_k, \dot{x}_k, y_k, \dot{y}_k, z_k, \dot{z}_k]^T$ is given by:

$$\mathbf{x}_k = \mathbf{x}_k^w - \mathbf{x}_k^{ws} \tag{1}$$

The radar sensor provides range, bearing, and range rate measurements, denoted as r_k, $\theta_k \in [-\pi, \pi]$, and $\dot{r}_k$ respectively, which are given by,

$$r_k = \sqrt{{x_k}^2 + {y_k}^2} \tag{2}$$

$$\theta_k = \tan^{-1}(y_k, x_k) \tag{3}$$

$$\dot{r}_k = \frac{(x_k \cdot \dot{x}_k + y_k \cdot \dot{y}_k)}{\sqrt{{x_k}^2 + {y_k}^2}} \tag{4}$$

The measurement vector of point P is denoted as $\mathbf{z}_k = [r_k, \theta_k, \dot{r}_k]^T$. The unit vector representing the radial direction of point P can be expressed as:

$$\mathbf{n} = (\cos\theta_k, \sin\theta_k, 0)^T \tag{5}$$

The velocity of the vehicle in the 2D plane at k^{th} time step are denoted as $\mathbf{v}_k^{wt} = [\dot{x}_k^{wt}, \dot{y}_k^{wt}]^T$ and $\mathbf{v}_k^t = [\dot{x}_k^t, \dot{y}_k^t]^T$ in the world and radar coordinate systems, respectively. The superscript t denotes the target vehicle. The orientation, $\gamma_k^{wt} \in [-\pi, \pi]$, and the relative orientation, $\gamma_k^t \in [-\pi, \pi]$, of the vehicle velocity are given by:

$$\gamma_k^{wt} = \tan^{-1}(\dot{y}_k^{wt}, \dot{x}_k^{wt}) \tag{6}$$

$$\gamma_k^t = \tan^{-1}(\dot{y}_k^t, \dot{x}_k^t) \tag{7}$$

The target local coordinate system (x, y, z) is another right-handed coordinate system defined for measurements from tires. Its origin is located at the tire center, from which the specific measurements comes from. The positive direction of its y axis is parallel to $\mathbf{v}_k^t$ but points forward. The angle between the y axis positive directions of the target local coordinate system and the reference coordinate system, denoted as $\phi \in [-\frac{\pi}{2}, \frac{\pi}{2}]$, can be expressed as:

$$\phi = \begin{cases} \gamma_k^t - \frac{\pi}{2}, & \gamma_k^t \in [0, \pi] \\ \gamma_k^t + \frac{\pi}{2}, & \gamma_k^t \in [-\pi, 0) \end{cases} \tag{8}$$

An example of the target local coordinate system is shown in Fig. 1.

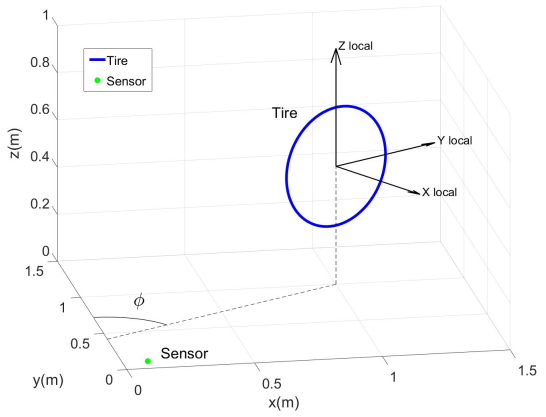

Fig. 1: Target local coordinate system

III. Doppler assisted L-fitting

Estimation of a bounding box for the target is usually performed with the location measurements and it aids in clustering as well. In the current work, the range rate measurements provided by the Doppler radar are used to provide a heading estimate for the target. The heading estimate combined with the location measurements can enhance the bounding box/ L fitting estimate.

A. Speed and Heading Estimation

In this section, a method to estimate the relative speed and heading using the bearing and Doppler measurements only from the body of the vehicles (i.e., no micro-Doppler) is proposed. The clustering method used to separate the micro-Doppler measurements and the measurements from the body is described in the first step of Section V. The heading estimate is later used in Section III-B to improve bounding box estimation.

For an arbitrary scattering point Q from the vehicle that is static relative to the vehicle, its Doppler shift is only induced by the translation of the vehicle. The translational Doppler shift can be calculated as

$$f_D = f_{Trans} = \frac{2f}{c}\mathbf{v}_k^t \cdot \mathbf{n} = \frac{2f}{c}|\mathbf{v}_k^t|\cos\left(\gamma_k^t - \theta_k\right) \tag{9}$$

where f is the operating frequency of the radar and c is the speed of light. Therefore the range rate for point Q is given by:

$$\dot{r}_k = \frac{c}{2f}\cdot f_D = \frac{c}{2f}\cdot f_D = |\mathbf{v}_k^t|\cos\left(\gamma_k^t - \theta_k\right) \tag{10}$$

The range of γ_k^t can be initially determined as:

$$\gamma_k^t \in \begin{cases} [\theta_k - \frac{\pi}{2}, \theta_k + \frac{\pi}{2}], & \dot{r}_k \geq 0 \\ [\theta_k - \pi, \theta_k - \frac{\pi}{2}) \cup (\theta_k + \frac{\pi}{2}, \theta_k + \pi], & \dot{r}_k < 0 \end{cases} \tag{11}$$

Assuming there are two known detection points Q_1 and Q_2 from the same vehicle and both static relative to the vehicle, their bearings are denoted as θ_k^{Q1} and θ_k^{Q2}, and their range rates are denoted as $\dot{r}_k^{Q1}$ and $\dot{r}_k^{Q2}$, respectively. Then according to Equation (10), the relative heading of the target speed can be estimated :

$$\hat{\gamma}_k^t = \tan^{-1}\Big(\dot{r}_k^{Q2}\cos\theta_k^{Q1} - \dot{r}_k^{Q1}\cos\theta_k^{Q2}, \dot{r}_k^{Q1}\sin\theta_k^{Q2} - \dot{r}_k^{Q2}\sin\theta_k^{Q1}\Big) \tag{12}$$

Then $|\mathbf{v}_k^t|$ can be estimated by:

$$|\hat{\mathbf{v}}_k^t| = \left|\frac{\dot{r}_k^{Q1}}{\cos\left(\hat{\gamma}_k^t - \theta_k^{Q1}\right)}\right| \tag{13}$$

Therefore, the relative heading and speed of a vehicle are observable with at least two known detections from its body.

The measurement equations of an arbitrary point Q_m from the vehicle body are given by:

$$\dot{r}^{Q_m} = |\mathbf{v}_k^t|\cdot\cos\left(\gamma_k^t - \theta_k^{Q_m}\right) + w_{\dot{r}} \tag{14}$$

$$\theta^{Q_m} = \theta_k^{Q_m} + w_\theta \tag{15}$$

in which $w_\theta \sim N(0, \sigma_\theta^2)$, $w_{\dot{r}} \sim N(0, \sigma_{\dot{r}}^2)$. Assuming that there are n known measurements from points $Q_1, Q_2, \ldots, Q_n$ on the vehicle body, the speed of the body $|\mathbf{v}_k^t|$, its heading γ_k^t and the azimuth angles $\theta_k^{Q_1}, \theta_k^{Q_2}, \ldots, \theta_k^{Q_n}$ are to be estimated. The measurement set $\mathbf{Z} = \left[\dot{r}^{Q_1}, \ldots, \dot{r}^{Q_n}, \theta^{Q_1}, \ldots, \theta^{Q_n}\right]^T$ can be written in terms of the parameters $\mathbf{x} = \left[\gamma_k^t, |\mathbf{v}_k^t|, \theta_k^{Q_1}, \ldots, \theta_k^{Q_n}\right]^T$ as

$$\mathbf{Z} = h(\mathbf{x}) + \mathbf{W}, \quad \mathbf{W} \sim \mathcal{N}(0, \mathbf{R}_n) \tag{16}$$

where $\mathbf{R}_n$ of size $2n \times 2n$ is the stacked covariance matrix $\mathbf{R}_n = \begin{bmatrix}\sigma_{\dot{r}}^2 I_n & 0 \\ 0 & \sigma_\theta^2 I_n\end{bmatrix}$. Linearizing (16) about a previous estimate (or an initial estimate) $\hat{\mathbf{x}}_{j-1}$ at the j^{th} iteration, the estimate $\hat{\mathbf{x}}_j$ for the current iteration can be found as

$$\mathbf{Z} = h(\hat{\mathbf{x}}_{j-1}) + \mathbf{H}\tilde{\mathbf{x}}_j + \mathbf{W} \tag{17}$$

$$\tilde{\mathbf{x}}_j = (\mathbf{H}^T\mathbf{R}_n^{-1}\mathbf{H})^{-1}\mathbf{H}^T\mathbf{R}_n^{-1}(\mathbf{Z} - h(\hat{\mathbf{x}}_{j-1})) \tag{18}$$

$$\hat{\mathbf{x}}_j = \hat{\mathbf{x}}_{j-1} + \tilde{\mathbf{x}}_j \tag{19}$$

where $\mathbf{H}$ is the Jacobian of the measurement function at the estimate $\hat{\mathbf{x}}$ (dropping the iteration index for ease of notation)

$$\mathbf{H} = \begin{bmatrix}\mathbf{H}_{\dot{r}} & \mathbf{H}_\theta\end{bmatrix} \tag{20}$$

$$\mathbf{H}_{\dot{r}} = \begin{bmatrix} -|\hat{\mathbf{v}}_k^t|\sin(\hat{\gamma}_k^t - \hat{\theta}_k^{Q_1}) & \cos(\hat{\gamma}_k^t - \hat{\theta}_k^{Q_1}) \\ \vdots & \vdots \\ -|\hat{\mathbf{v}}_k^t|\sin(\hat{\gamma}_k^t - \hat{\theta}_k^{Q_n}) & \cos(\hat{\gamma}_k^t - \hat{\theta}_k^{Q_n}) \\ 0 & 0 \\ \vdots & \vdots \\ 0 & 0 \end{bmatrix} \tag{21}$$

$$\mathbf{H}_\theta = \begin{bmatrix}\mathrm{diag}(|\hat{\mathbf{v}}_k^t|\sin(\hat{\gamma}_k^t - \hat{\theta}_k^{Q_1}), \ldots, |\hat{\mathbf{v}}_k^t|\sin(\hat{\gamma}_k^t - \hat{\theta}_k^{Q_n})) \\ I_n\end{bmatrix} \tag{22}$$

The iterations continue till the difference in the estimates is below a threshold or a maximum number of iterations is reached.

To evaluate the dispersion in the estimates, the Cramér–Rao lower bound (CRLB), which is the lower bound of the variance of the estimates, can be calculated. The CRLB matrix is expressed as $\rho = \mathbf{J}^{-1}$, in which $\mathbf{J}$ is the Fisher information matrix that measures the amount of information that the detections carry about the relative heading and speed, given by

$$\mathbf{J} = H^T R_n^{-1} H \tag{23}$$

where H is the Jacobian calculated using the true parameters. It can be shown that $\mathbf{J}$ is invertible only when $n \geq 2$, which means the relative heading and speed are observable only in this case. Since the true parameters are not available, the $\mathbf{J}$ and the corresponding ρ are calculated using the estimate at the final iteration, and ρ is used as the covariance of the estimate. In the current work, estimation is performed at each time step using only the measurements at the current time step and the information from previous time steps is not used. However, the speed and heading estimates, along with their uncertainties, can be used for further tracking applications.

B. L Fitting

Given the locations of the n measurements (converted Cartesian measurements) of a cluster and an estimate of the heading, the objective is to determine the length and width of the bounding box/L shape that fits the measurements, while refining the heading estimate.

For a given heading estimate $\hat{\gamma}$, the projections of each measurement $\begin{bmatrix} z_x^m & z_y^m \end{bmatrix}^T$, $m = 1$ to n, are calculated along the direction of the heading and perpendicular to the direction of the heading.

$$\begin{bmatrix} z_\gamma^m \\ z_{\gamma^\perp}^m \end{bmatrix} = \begin{bmatrix} \cos(\hat{\gamma}) & \sin(\hat{\gamma}) \\ -\sin(\hat{\gamma}) & \cos(\hat{\gamma}) \end{bmatrix} \begin{bmatrix} z_x^m \\ z_y^m \end{bmatrix} \tag{24}$$

As in the real data distribution and experiments, each of the measurement projection components in L-shape clusters approximately follows the exponential distribution. Therefore, each component of the projections is made non-negative by shifting them to $(0, +\infty)$, which is notated as $z_{\gamma s}^m$ and $z_{\gamma^\perp s}^m$, and the likelihood function of each of the component is fit as follows

$$\lambda_\gamma = \arg\max_\lambda \prod_{m=1}^{n} \frac{1}{\lambda} e^{-\lambda z_{\gamma s}^m} \tag{25}$$

$$\lambda_{\gamma^\perp} = \arg\max_\lambda \prod_{m=1}^{n} \frac{1}{\lambda} e^{-\lambda z_{\gamma^\perp s}^m} \tag{26}$$

The log of the posterior distribution L_p for $\hat{\gamma}$ can be calculated using the prior distribution of γ from III-A and the likelihood of the measurements

$$L_p = \log \Bigg[\mathcal{N}(\hat{\gamma}; \bar{\gamma}, \sigma_\gamma^2) + \sum_{m=1}^{n} \max\Big(\log\Big(\frac{1}{\lambda_\gamma} e^{-\lambda_\gamma z_{\gamma s}^m}\Big), \log\Big(\frac{1}{\lambda_{\gamma^\perp}} e^{-\lambda_{\gamma^\perp} z_{\gamma^\perp s}^m}\Big)\Big) \Bigg] \tag{27}$$

The log posterior is calculated for values $\hat{\gamma} = \bar{\gamma} - 3\sigma_{\hat{\gamma}}$ to $\bar{\gamma} + 3\sigma_{\hat{\gamma}}$ in steps of $\delta\gamma$ and the value that maximizes the log posterior is chosen as the refined heading estimate. The length and width are estimated as the difference between the maximum and minimum of the projections in each of the directions:

$$\hat{l} = \max(\mathbf{z}_\gamma) - \min(\mathbf{z}_\gamma) \tag{28}$$

$$\hat{w} = \max(\mathbf{z}_{\gamma^\perp}) - \min(\mathbf{z}_{\gamma^\perp}) \tag{29}$$

where $\mathbf{z}_\gamma$ and $\mathbf{z}_{\gamma^\perp}$ contains the projection component from all the measurements.

IV. Effect of Micro Doppler

The micro-motion of a part of the target may introduce additional Doppler modulation in measurements and produce range rate error. In this section, the effect of micro-Doppler induced by rotation of vehicle tires is discussed and formulated to handle the micro-Doppler effect in autonomous driving scenario.

A. Range Rate Equation Considering Micro Doppler Effect

The target tire rotates about the x axis in the yoz plane in the target local coordinate system. Assume the vehicle moves toward the radar, so the tire rotates in the x-axis positive direction defined by the target local coordinate system. Since the scalar linear velocity of the outermost points on the tire is the same as the scalar linear velocity of the vehicle, the angular velocity ω is given by:

$$\omega = (\omega_x, \omega_y, \omega_z)^T = \left(\frac{|\mathbf{v}_k^{wt}|}{R}, 0, 0\right)^T \tag{30}$$

in which R is the radius of the tire.

The location of an arbitrary point P at a distance $L \in [0, R]$ from the tire center and that forms an angle ψ at the k-th time step can be written in target local coordinate system as $\boldsymbol{r}_P = \begin{bmatrix} 0 & L\sin(\psi) & L\cos(\psi) \end{bmatrix}^T$. $\boldsymbol{R}_{init}$ is a rotation matrix that transforms coordinates in the target local coordinate system to coordinates in the radar coordinate system, given by:

$$\boldsymbol{R}_{init} = \begin{bmatrix} \cos\phi & -\sin\phi & 0 \\ \sin\phi & \cos\phi & 0 \\ 0 & 0 & 1 \end{bmatrix} \tag{31}$$

According to [10], the micro-Doppler frequency shift induced by the rotation of the target tire is demonstrated by:

$$\begin{aligned} f_{mD} &= \frac{2f}{c}[\boldsymbol{R}_\phi(\omega \times \boldsymbol{r}_P)] \cdot \mathbf{n} \\ &= \frac{2fL|\mathbf{v}_k^{wt}|}{Rc} \sin(\phi - \theta_k) \sin\psi \end{aligned} \tag{32}$$

The Doppler shift of point *P* is demonstrated by:

$$f_D = f_{Trans} + f_{mD} \tag{33}$$

where f_{Trans} is the Doppler shift induced by the translation of the target tire, given by Equation (9).

Therefore, according to equation (8) and (32), the Doppler shift of point P is given by:

$$f_D = \begin{cases} \frac{2f\cos(\gamma_k^t-\theta_k)}{c}(|\mathbf{v}_k^t| - |\mathbf{v}_k^{wt}| \cdot \frac{L}{R}\sin\psi), \\ \gamma_k^t \in [0,\pi] \\ \frac{2f\cos(\gamma_k^t-\theta_k)}{c}(|\mathbf{v}_k^t| + |\mathbf{v}_k^{wt}| \cdot \frac{L}{R}\sin\psi), \\ \gamma_k^t \in [-\pi,0) \end{cases} \tag{34}$$

Then the radial velocity measurement from arbitrary point P can also be expressed as:

$$\dot{r}_k = \begin{cases} \cos(\gamma_k^t-\theta_k)(|\mathbf{v}_k^t| - |\mathbf{v}_k^{wt}| \cdot \frac{L}{R}\sin\psi), & \gamma_k^t \in [0,\pi] \\ \cos(\gamma_k^t-\theta_k)(|\mathbf{v}_k^t| + |\mathbf{v}_k^{wt}| \cdot \frac{L}{R}\sin\psi), & \gamma_k^t \in [-\pi,0) \end{cases} \tag{35}$$

B. Probability Distribution of Range Rate

For a tire of radius R, the conditional cumulative density of distance L from the tire center is given by

$$P_{L|R}(l) = P_{L|R}(L \le l) = \frac{l^2}{R^2} \tag{36}$$

Then the conditional probability density function of L is given by:

$$p_{L|R}(l) = \frac{\partial P_{L|R}(l)}{\partial l} = \frac{2l}{R^2}, \quad l \in [0,R] \tag{37}$$

Define $X = \frac{L}{R}$, the probability density function of X is given by:

$$p_X(x) = \int_{-\infty}^{+\infty} |r| \cdot p_{L,R}(xr, r)dr = 2x, x \in [0,1] \tag{38}$$

Define $Y = \sin\psi$, then $\psi = g(Y) = \sin^{-1} y$. The conditional probability density function of Y is given by:

$$p_Y(y) = p_\theta(g(y)) \cdot |g'(y)| = \frac{1}{2\pi\sqrt{1-y^2}}, \quad y \in [-1,1] \tag{39}$$

The probability density function of $Z = XY$ can be calculated by:

$$p_Z(z) = \frac{\sqrt{1-z^2}}{\pi}, z \in [-1,1] \tag{40}$$

$\dot{r}_k$ is given by:

$$\dot{r}_k = \begin{cases} \cos(\gamma_k^t-\theta_k)(|\mathbf{v}_k^t| - |\mathbf{v}_k^{wt}| \cdot Z), & \gamma_k^t \in [0,\pi] \\ \cos(\gamma_k^t-\theta_k)(|\mathbf{v}_k^t| + |\mathbf{v}_k^{wt}| \cdot Z), & \gamma_k^t \in [-\pi,0) \end{cases} \tag{41}$$

The probability density function of $\dot{r}_k$ can be expressed as:

$$\begin{aligned} &p_{\dot{r}_k}(a) = p_Z(h(a))|h'(a)| \\ &= \frac{2}{\pi|\mathbf{v}_k^{wt}|^2\cos^2(\gamma_k^t-\theta_k)} \cdot \\ &\sqrt{|\mathbf{v}_k^{wt}|^2\cos^2(\gamma_k^t-\theta_k) - (a - |\mathbf{v}_k^t|\cos(\gamma_k^t-\theta_k))^2} \end{aligned} \tag{42}$$

The range of $\dot{r}_k$ is given by:

$$\begin{aligned} \dot{r}_k \in [&|\mathbf{v}_k^t|\cos(\gamma_k^t-\theta_k) - |\mathbf{v}_k^{wt}||\cos(\gamma_k^t-\theta_k)|, \\ &|\mathbf{v}_k^t|\cos(\gamma_k^t-\theta_k) + |\mathbf{v}_k^{wt}||\cos(\gamma_k^t-\theta_k)|] \end{aligned} \tag{43}$$

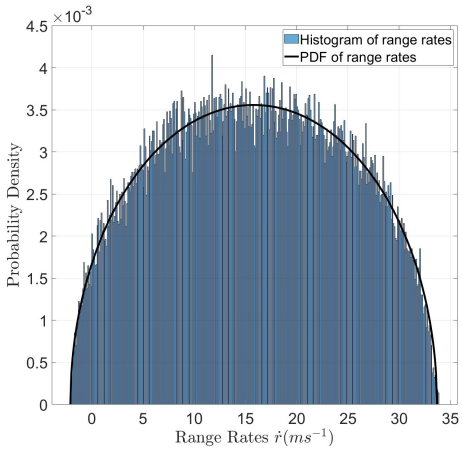

Fig. 2: Histogram of micro-Doppler range rate samples overlaid with calculated p.d.f

The mean of $\dot{r}$ is given by:

$$E(\dot{r}) = |\mathbf{v}_k^t| \cdot \cos(\gamma_k^t - \theta_k) \tag{44}$$

The variance of $\dot{r}$ is given by:

$$var(\dot{r}) = \frac{|\mathbf{v}_k^{wt}|^2|\cos(\gamma_k^t-\theta_k)|^2}{4} \tag{45}$$

Fig. 2 shows the histogram of range rate samples and the probability density calculated using Equation (42) for a target with $|\mathbf{v}_k^{wt}| = 18ms^{-1}, |\mathbf{v}_k^t| = 15.89ms^{-1}, \gamma_k^t = 47.54°$ and $\theta_k = 53.74°$

V. Two-step Clustering

The objective of the clustering is to group the measurements from the body and the tires of the same target, while separating the measurements from different targets. While closely spaced targets with different velocities can be distinguished using Doppler measurements, this process is challenging in presence of micro-Doppler since the measurements from the same target can have different range rates while being close in distance/range. In this section, a two-step clustering method combining Doppler-assisted bounding box estimation method mentioned in III is proposed as shown in Fig. 3, which can be divided into the following steps:

1) The 2D Doppler radar measurements are preliminarily clustered based on the distance and range rate difference between every two points. The clustering threshold for range rate difference is relatively small, so each cluster will only contain either measurements from the vehicle bodies or measurements from the rotating tires.
2) Sort the clusters in the descending order of cluster size, such that the larger clusters that are more likely to contain detections from the vehicle bodies are traversed first in the subsequent merging of clusters.
3) Traverse through each cluster in the above-mentioned order to merge relevant clusters. For each cluster:
   a) If the cluster is traversed for the first time, estimate the relative speed $\hat{s}$ and heading $\hat{\gamma}$ of the

corresponding target using the proposed estimation method in III-A, then the real speed of the target also can be estimated as $\hat{v}$. The standard deviation of estimation $\sigma_{\hat{s}}$ and $\sigma_{\hat{\gamma}}$ is also given by calculating the CRLB of estimation.

b) Estimate the exact heading, length, and width of the corresponding target by performing MAP L-fitting mentioned in III-B on the cluster.

c) A measurement from other clusters is merged into this cluster if the following criteria are satisfied:

i) *Criterion 1:* The range rate of the measurement falls in the interval given by Equation (43), which implies it could be a measurement from the tire of the same vehicle. Considering the error in the estimates, the interval is modified to

$$\dot{r}_k \in [\max(\hat{s}-3\sigma_{\hat{s}},0)\cos(\hat{\gamma}-\theta_k)-\hat{v}|\cos(\hat{\gamma}-\theta_k)|, (\hat{s}+3\sigma_{\hat{s}})\cos(\hat{\gamma}-\theta_k)+\hat{v}|\cos(\hat{\gamma}-\theta_k)|] \tag{46}$$

This criterion is only considered when the estimation of relative speed is accurate, i.e. $\sigma_{\hat{s}} \leq \epsilon_s$, in which ϵ_s is a preset threshold.

ii) *Criterion 2:* The estimated length $\hat{l}$ and width $\hat{w}$ of the cluster after containing it are smaller than preset thresholds considering measurement noise:

$$\hat{l} \leq \epsilon_l + e_l \quad \cap \quad \hat{w} \leq \epsilon_w + e_w \tag{47}$$

in which ϵ_l and ϵ_w are preset thresholds set to the maximum length and width of the target, and e_l and e_w are the approximate errors produced by measurement noise:

$$e_l = 3\sigma_\theta(r_k+3\sigma_r)\left|\cos\left(\theta_k-\frac{\pi}{2}-\hat{\gamma}\right)\right| \tag{48}$$

$$e_w = 3\sigma_\theta(r_k+3\sigma_r)\left|\sin\left(\theta_k-\frac{\pi}{2}-\hat{\gamma}\right)\right| \tag{49}$$

4) The clusters are merged (if possible) iteratively by repeating the above-mentioned steps 3b-3c until the clustering results remain unchanged.

VI. Results

A. CRLB of speed and heading estimation

To evaluate the performance of the speed and heading estimation algorithm in Subsection III-A, the CRLB and RMSE are calculated and compared in MATLAB simulation. Fig. 4 shows the scenario of the simulation. As shown in Fig. 4, the sensor is located at the origin, and a rectangular target is located on the x-axis with different headings and ranges. Range rate and azimuth measurements randomly generated from the target body according to the Equation (14)-(15) are used as inputs for the simulation. The RMSE and CRLB of the proposed algorithm under different scenarios are shown in Table I. As shown in Table I, the RMSE values of the

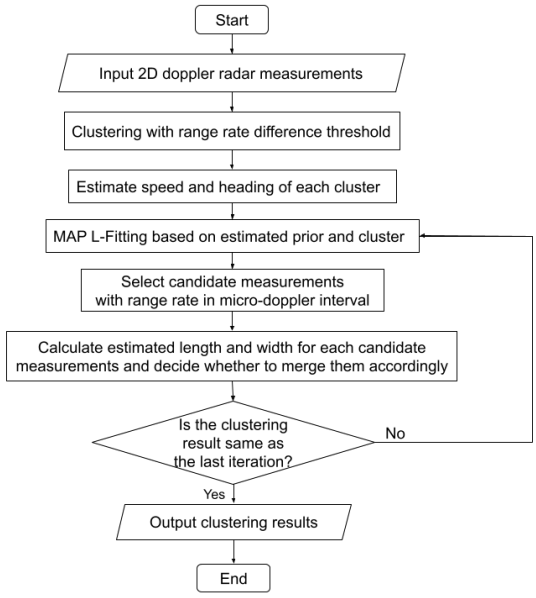

Fig. 3: Flowchart of proposed two-step clustering algorithm

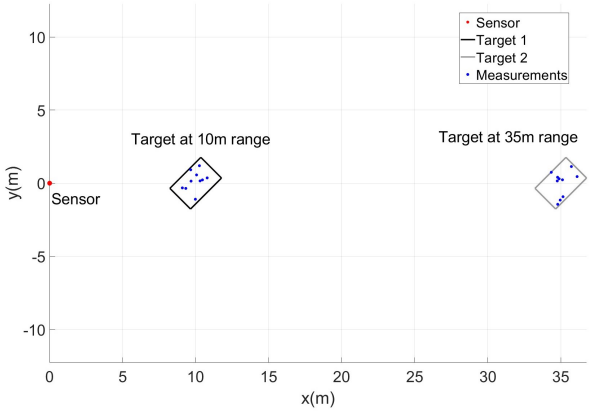

Fig. 4: Scenario used for CRLB of speed and heading

TABLE I: CRLB and RMSE of the estimated heading and speed.

range (m)	$\gamma(^\circ)$	$\hat{\gamma}(^\circ)$		$\hat{s}(m/s)$	
		CRLB	RMSE	CRLB	RMSE
10	0	0.68	0.69	0.03	0.03
	15	1.48	1.50	0.39	0.40
	30	1.13	1.13	0.52	0.52
	45	1.27	1.28	1.04	1.05
	60	1.45	1.44	2.20	2.22
	75	0.60	0.60	1.83	1.82
	90	0.22	0.22	2.48	2.52
35	0	2.15	2.74	0.03	0.20
	15	3.28	3.77	0.76	1.10
	30	3.77	3.94	1.91	2.25
	45	6.45	6.79	5.63	8.64
	60	3.46	3.48	5.28	5.88
	75	1.97	1.98	6.38	6.98
	90	0.19	0.19	6.38	6.84

proposed algorithm are very close to the CRLB values of the measurement model when the target is near the sensor. As the target moves further away, the gap between CRLB and RMSE values increases due to a decrease in the geometric diversity of measurements, i.e., far away targets produce a smaller range of azimuth measurements. Overall, the RMSE is close to the CRLB under various conditions, which proves the estimation accuracy and applicability of our proposed speed and heading estimation algorithm.

B. MAP L-fitting

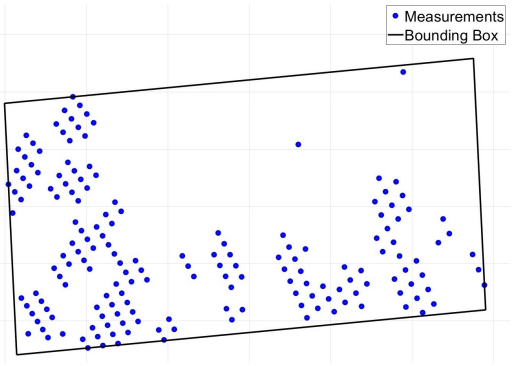

Fig. 5: Results for MAP L-fitting

To evaluate the performance of the maximum a posteriori (MAP) L-fitting method proposed in subsection III-B, this method is compared with other methods using closeness and variance criteria in [9] on 41 vehicle scanning point clusters, manually selected from 298 frames of data recorded in 29.71s. 32 of the clusters are near and complete L-shaped clusters from targets within 20m, and the remaining 18 clusters are far and incomplete clusters from targets 20-40m away. For the proposed method, the prior distribution of heading is set as a normal distribution with a mean of 0° and a standard derivation of 3.77°. The RMSE for the heading, the length l, and the width w are shown in Table II and Table III. The sample is as shown in Figure 5.

TABLE II: RMSE for close-by target and complete clusters

Method	$RMSE_\gamma(^\circ)$	$RMSE_l$(m)	$RMSE_w$(m)
Closeness criterion	29.82	0.3768	1.2956
Variance criterion	3.938	0.0249	0.0643
MAP (proposed)	1.507	0.0147	0.0277

TABLE III: RMSE for far away target and incomplete clusters

Method	$RMSE_\gamma(^\circ)$	$RMSE_l$(m)	$RMSE_w$(m)
Closeness criterion	28.98	0.3885	0.9702
Variance criterion	12.92	0.1346	0.1931
MAP (proposed)	4.791	0.0675	0.1472

As in Table II and Table III, although the errors of our proposed MAP L-fitting method increase as the target moves further away, our proposed method still outperforms the two other methods in different real scenarios.

C. Clustering Results

To evaluate the performance of our proposed clustering method, the following clustering methods are compared:

1) Classical DBSCAN method [4] that only considers the Euclidean distance metric. Since the contribution of the proposed method is to improved clustering with Doppler information, the clustering method can also be switched to other more advanced algorithm, e.g. HDBSCAN.
2) Doppler-assisted DBSCAN: DBSCAN method that considers both the Euclidean distance metric and range rate differences.
3) Our proposed two-step clustering method.

The clustering methods are tested in the following scenarios in which the measurements may be merged into a wrong cluster (referred to as merging error) or erroneous extra clusters are produced (referred to as splitting error) -

1) Scenario 1: Measurements come from two vehicles with different relative velocities to the sensor, which are close to each other in some frames, and there are no measurements from the tires (see Fig. 6a).
2) Scenario 2: Measurements come from two vehicles with different relative velocities to the sensor, which are close to each other in some frames, and there are some measurements from the tires (see Fig. 6b).
3) Scenario 3: Measurements come from two vehicles close to each other, with the same relative velocities to the sensor, and there are some measurements from the tires (see Fig. 6c).

The performances of different clustering methods in Scenario 1 are shown in Table IV. From the results of Table IV, utilizing Doppler information in clustering can minimize the merging errors and significantly increase the clustering accuracy when the extended targets are close to each other. Compared with the Doppler-assisted DBSCAN, our proposed method further improved the clustering accuracy by combining the bounding box estimation, although some nearby noise points are merged into the cluster and the merging error is slightly increased.

Table V shows the clustering performance of different algorithms in Scenario 2. When there are measurements from the tires of the vehicles, the Doppler-assisted method suffers from severe splitting error due to the micro-Doppler effect. Our proposed algorithm maintains a high accuracy compared to the other methods, and it significantly reduces the splitting error caused by the micro-Doppler effect.

If measurements come from two close-by vehicles with the same relative velocities as the sensor, the proposed method is unable to achieve high performance since the measurements from different targets are similar in both range rate and position. Table VI shows the evaluation of clustering results in this kind of scenario. Compared with the other 2 scenarios, the performance of our proposed method drops sharply, but still outperforms the other two clustering methods in clustering accuracy.

Overall, the proposed clustering algorithm outperforms the

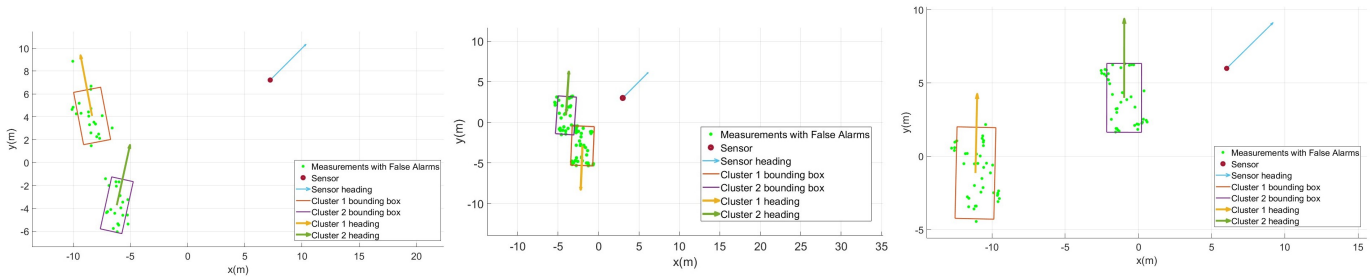

(a) Scenario 1 (b) Scenario 2 (c) Scenario 3

Fig. 6: Scenarios used for clustering

TABLE IV: Performance evaluations in Scenario 1

Metric	Classical DBSCAN	Doppler-assisted DBSCAN	Proposed Clustering method
Correct clustering (%)	80.20	88.65	91.04
Average splitting error	0.54	0.81	0.81
Average merging error	0.54	0.21	0.43

TABLE V: Performance evaluations in Scenario 2

Metric	Classical DBSCAN	Doppler-assisted DBSCAN	Proposed Clustering method
Correct clustering (%)	83.61	39.68	87.31
Average splitting error	4.15	35.26	4.11
Average merging error	0.12	0.05	0.11

TABLE VI: Performance evaluations in Scenario 3

Metric	Classical DBSCAN	Doppler-assisted DBSCAN	Proposed Clustering method
Correct clustering (%)	60.18	50.95	70.32
Average splitting error	0.18	14.50	5.56
Average merging error	0.93	1.39	1.79

other methods in most of the scenarios, which shows its robustness and accuracy in various conditions with or without the micro-Doppler effect.

VII. Conclusion

In this paper, the inclusion of Doppler measurements for bounding box estimation and clustering was addressed. Specifically, the bounding box and clustering performance were improved by including the Doppler measurements while reducing the negative effect of micro-Doppler due to tire rotation. A nonlinear iterative least squares method was developed for estimating the heading and speed of each cluster, and this heading estimate was used in constructing the bounding box using MAP L-fitting, using only the measurements corresponding to the target body. These estimates are then used to iteratively refine the clusters to include other measurements from the same target while maintaining the measurements from the body and tires separately.

Currently, the estimation and clustering are done frame by frame, considering a single frame at a time. Tracking the target over time frames by extending the proposed approach is a direction for future work.

References

[1] P. Li, P. Wang, K. Berntorp, and H. Liu, "Exploiting temporal relations on radar perception for autonomous driving," in *Proceedings of the IEEE/CVF Conference on Computer Vision and Pattern Recognition (CVPR)*, June 2022, pp. 17 071–17 080.

[2] M. Kumar and S. Mondal, "Recent developments on target tracking problems: A review," *Ocean Engineering*, vol. 236, p. 109558, 2021.

[3] Y. Bar-Shalom, P. K. Willett, and X. Tian, *Tracking and data fusion: A handbook of algorithms*. YBS publishing Storrs, 2011, vol. 11.

[4] M. Ester, H.-P. Kriegel, J. Sander, X. Xu *et al.*, "A density-based algorithm for discovering clusters in large spatial databases with noise." in *2nd International Conference on Knowledge Discovery and Data Mining (KDD)*, vol. 96, no. 34, 1996, pp. 226–231.

[5] J. Zeng, J. Wang, L. Guo, G. Fan, K. Zhang, and G. Gui, "Cell scene division and visualization based on autoencoder and k-means algorithm," *IEEE Access*, vol. 7, pp. 165 217–165 225, 2019.

[6] N. Scheiner, N. Appenrodt, J. Dickmann, and B. Sick, "A multi-stage clustering framework for automotive radar data," in *2019 IEEE Intelligent Transportation Systems Conference (ITSC)*, 2019, pp. 2060–2067.

[7] T. Wagner, R. Feger, and A. Stelzer, "Modification of dbscan and application to range/doppler/doa measurements for pedestrian recognition with an automotive radar system," in *2015 European Radar Conference (EuRAD)*, 2015, pp. 269–272.

[8] C. Kuang, C. Wang, B. Wen, and W. Huang, "An applied method for clustering extended targets with uhf radar," *IEEE Access*, vol. 8, pp. 98 670–98 678, 2020.

[9] X. Zhang, W. Xu, C. Dong, and J. M. Dolan, "Efficient l-shape fitting for vehicle detection using laser scanners," in *2017 IEEE Intelligent Vehicles Symposium (IV)*, 2017, pp. 54–59.

[10] V. C. Chen, *The micro-Doppler effect in radar*. Artech house, 2019.

[11] T. Wagner, R. Feger, and A. Stelzer, "A fast grid-based clustering algorithm for range/doppler/doa measurements," in *2016 European Radar Conference (EuRAD)*, 2016, pp. 105–108.